



Microstructure and mechanical properties of friction stir welded full annealing condition Al-Cu-Li alloys

Ge Liu^a, Meizi Tian^a, Peng Chen^{b,*}, Jie Wang^b, Wenhao Chen^b, Zhiqing Zhang^c

^a School of Robot Engineering, Yangtze Normal University, Chongqing 408100, China

^b School of New Energy and Materials, Southwest Petroleum University, Chengdu 610500, China

^c College of Materials Science and Engineering, Chongqing University, Chongqing 400045, China

ARTICLE INFO

Keywords:

Annealed condition Al-Cu-Li alloy
Friction stir welding
Microstructure
Phase
Mechanical properties

ABSTRACT

The paper focuses on the friction stir welding (FSW) of Al-Cu-Li alloy in the fully annealed condition, with particular attention to its local microstructural evolution and mechanical properties. It was observed that nugget zones exhibit finely equiaxed grains resulting from sufficient dynamic recrystallization (DRX), primarily occurring through continuous dynamic recrystallization (CDRX) and discontinuous dynamic recrystallization (DDRX). In the thermo-mechanically affected zone (TMAZ), numerous equiaxed grains and sub-structured grains emerged due to partial DRX, indicating the development of CDRX, DDRX, and geometric dynamic recrystallization (GDRX). The precipitate characteristics of the heat affected zone (HAZ), TMAZ, and base material (BM) are fundamentally consistent, specifically, there exists a significant amount of coarse equilibrium phases at grain boundaries, which exhibit relatively low hardness. The microhardness values of the nugget zone (NZ) and HAZ are comparable, exhibiting the lowest hardness region in the welded joint, with an average value of approximately 50.5 HV. These equilibrium phases predominantly undergo dissolution within the NZ, exhibiting a marked solid solution strengthening effect that enhances hardness, with a peak value reaching 125.2 HV. From advancing side to retreating side of the NZ, dissolution of the phases gradually decreases, leading to a sequential reduction in solid solution strengthening effects across these three regions. Consequently, the increment in hardness diminishes progressively, with a minimum hardness of about 69.8 HV, resulting in a 'n'-shaped distribution of overall joint hardness. The FSW joints exhibit a maximum tensile strength of 179.9 MPa, corresponding to approximately 95.0 % of the BM, while the elongation at fracture reaches 13.4 %, representing 68.7 % of the BM. Both tensile fracture surfaces for the joints and BM reveal numerous dimples indicative of ductile fracture characteristics. However, the joints exhibit lower uniform deformation capability compared to base materials, indicating that their post-fracture elongation is less than that of the BM.

1. Introduction

In recent years, with the rapid development of modern industries such as aerospace, automotive, and marine engineering, the demand for lightweight and high-strength structural materials has been growing at an astonishing pace [1]. This upsurge is mainly propelled by the urgent requirements to reduce fuel consumption in transportation-related fields. The Al-Cu-Li alloy, with its unique combination of low density and outstanding strength properties, has emerged as a star material in the aerospace industry. For instance, adding only 1 % lithium to an aluminum matrix can lead to a remarkable 3 % decrease in density and a 6 % increase in elasticity simultaneously [2,3]. This makes it an ideal

choice for manufacturing aircraft components such as wing spars, fuselage frames, and engine parts. These components need to be lightweight to reduce the overall weight of the aircraft while maintaining high strength to withstand the complex mechanical stresses during flight [4].

In 1991, Thomas from The Welding Institute (TWI, UK) made a groundbreaking invention - the inclined Friction Stir Welding (FSW), which is a highly complex thermomechanical process [3]. This technology typically operates at a temperature around 0.6–0.9 T_m (Kelvin). Such a temperature range is carefully chosen because it is beneficial for avoiding the common drawbacks of traditional fusion welding. In fusion welding, issues like porosity, hot cracking, and large-scale grain growth

* Corresponding author.

E-mail address: xd_chenpeng@163.com (P. Chen).

<https://doi.org/10.1016/j.mtcomm.2025.113399>

Received 9 February 2025; Received in revised form 4 July 2025; Accepted 23 July 2025

Available online 24 July 2025

2352-4928/© 2025 Elsevier Ltd. All rights are reserved, including those for text and data mining, AI training, and similar technologies.

often occur, which can severely degrade the mechanical properties of the welded joints [5]. In contrast, FSW, with its unique frictional heating and plastic deformation mechanism, can produce high-quality welds with fewer defects. Therefore, it is widely considered an ideal welding technique for Al alloys [4]. Previous studies have shown that FSW can be effectively used in the manufacturing of Al-Cu-Li alloys [6–8]. Moreover, different welding parameters, such as rotation speed, welding speed, and axial force, will result in a complex microstructure and precipitation behaviors. These variations significantly affect the mechanical properties of the joints, including tensile strength, fatigue resistance, and corrosion resistance [9–11].

FSW joints generally consist of distinct zones: the nugget zone (NZ), the thermo-mechanical affected zone (TMAZ), the heat-affected zone (HAZ), and the base material (BM). These regions are characterized by distinct heterogeneities in plastic deformation and thermal exposure [12]. During the FSW process, the joints experience significant changes, leading to the generation of Dynamic Recrystallization (DRX) [13,14]. Generally, several types of DRX can be observed during FSW, including discontinuous dynamic recrystallization (DDR), continuous dynamic recrystallization (CDRX), and geometric dynamic recrystallization (GDRX) [15]. In DDR, new strain-free grains nucleate and grow at the expense of dislocation-rich regions [16]. The nucleation process is related to the local stress concentration and the stored energy in the deformed material [13]. Deformation, facilitated by dynamic recovery, results in the formation of cell or sub-grain structures with low-angle grain boundaries (LAGBs) [16]. As the deformation progresses, the sub-grain boundaries gradually accumulate dislocations. Under higher deformations, the progressive evolution of these LAGBs into high-angle grain boundaries (HAGBs) is the characteristic of CDRX. GDRX can be observed in extensive high-temperature aluminum deformations, where the grains elongate and show local serrations. These grains remain distinct until their thickness is less than one or two sub-grain sizes. Beyond this, the formed serrations disappear, and equiaxed grains marked by HAGBs are formed. It has been demonstrated that complete DRX occurs in the NZ, while partial DRX occurs in the TMAZ due to differences in the degree of plastic deformation and welding temperatures [16]. In addition, the HAZ mainly undergoes recovery due to thermal cycling, resulting in negligible changes in grain morphology or size [13]. Currently, the dominant recrystallization mechanisms in distinct characteristic regions of FSW joints remain insufficiently explored. This is particularly true for annealing condition Al-Cu-Li alloys, where a systematic analysis of recrystallization behavior across microstructural zones could elucidate the material's deformation mechanisms under complex thermomechanical processing conditions.

The Al-Cu-Li alloy is a typical precipitation-hardening Al alloy with a complex precipitation system, including the Guinier-Preston Zones (GPZs), θ' , θ , δ' , β' , T_1 , T_2 , and possibly Ω and S' as well [2]. The precipitates in the FSW joints of this alloy have been extensively studied [17–19]. During the FSW of Al-Cu-Li alloys, complex precipitation behaviors such as dissolution, coarsening, precipitation, and re-precipitation occur. It should be noted that most of the conclusions about precipitation behaviors are obtained from the artificially aged (T8/T6) Al-Cu-Li alloy. For example, Sun et al. studied the microstructure, mechanical, and fracture properties of FSWed joints in 2195-T8 Al-Li alloy [4]. They used advanced characterization techniques like high-resolution transmission electron microscopy (HRTEM) and atom probe tomography (APT) to analyze the fine-scale microstructure and the distribution of precipitates. Guo et al. investigated the effect of aging treatment on the microstructure and mechanical properties of the welded joints of 2195-T8 Al-Li alloy [20]. Their research involved a series of aging experiments at different temperatures and times, followed by mechanical property tests such as tensile testing and hardness measurement. However, only a few researchers have focused on other temper conditions of the Al-Cu-Li alloy. Mondal et al. reported the effect of the backing plate on the microstructure and properties of friction-stir-welded 2195-O Al alloy [21]. They varied the material and

thickness of the backing plate to study its influence on the heat dissipation and the resulting microstructure. Chen et al. studied the joint performance of friction-stir-welded 2195-O Al-Li alloy through post-weld heat treatment [22]. Their study included different heat-treatment cycles to optimize the mechanical properties of the joints. Chen et al. also explored the influence of post-weld rolling and artificial aging on the microstructure and mechanical properties of friction-stir-welded 2195-T4 Al-Li alloy joints [23]. Their work involved multi-step processing and comprehensive characterization to understand the complex relationships between processing, microstructure, and properties. The precipitation evolution and mechanical properties of FSW joints based on different temper conditions of Al-Cu-Li alloy are different and still not fully understood.

In engineering, the fully annealed (O condition) aluminum alloy is mainly used for the processing of special profiles. After deformation, welding, and other cold/hot processing, appropriate heat treatment is carried out to prepare parts with good comprehensive performance. The alloy in this heat-treatment condition has been annealed at a high temperature for a long time, so most of the solute atoms in the alloy precipitate into soft and coarse precipitates, and the hardness of the alloy is low. This soft state makes it easier to form complex shapes during cold-rolling or forging processes. Nevertheless, the friction stir welding of fully annealed Al-Cu-Li alloy has received little attention, and the microstructure evolution and mechanical properties of the joints are not very clear. There is a lack of systematic research on how the initial soft state of the alloy affects the FSW process, the resulting microstructure, and the mechanical properties of the joints.

To gain a deeper understanding of this issue, the present study mainly investigated the microstructure and mechanical properties of friction-stir-welded fully annealed Al-Cu-Li alloy and revealed the relationships among the grain features, precipitates, hardness, and tensile properties of the FSW joints. To achieve this goal, a series of advanced techniques were employed. Optical microscope (OM) was used to observe the overall microstructure and the distribution of different zones in the FSW joints. Back-scattered electron (BSE) imaging provided information about the chemical composition and the distribution of precipitates at a higher magnification. Electron back-scattered diffraction (EBSD) was utilized to analyze the crystallographic orientation and the grain boundary characteristics, such as the misorientation angle between grains. Transmission electron microscopy (TEM) was applied to study the fine-scale microstructure, including the size, shape, and distribution of precipitates. Vickers hardness testers were used to measure the hardness distribution across different zones of the joints, and tensile test machines were employed to measure the tensile properties.

2. Experiment work

In this study, the base material (BM) was in a Al-Cu-Li alloy plate (4 wt% Cu, 1 wt% Li, 0.44 wt% Mg, 0.4 wt% Ag, 0.11 wt% Zr, 0.05 wt% Fe) with fully annealed condition, which was annealed at 400 °C more than 24 h. The BM were manufactured by friction stir butt welding with a rotation speed of 700 rpm and a welding speed of 100 mm/min. The welding procedure was performed perpendicular to the rolling direction (RD) of the BM with the shoulder plunge depth of 0.1 mm and the tool tilt angle of 2.5°. A FSW tool is made of high-speed steel and consists of a concave shoulder with 18 mm in diameter and a threaded taper cylindrical pin with 6.9 mm in length.

After welding, microstructure of the FSW joints was conducted on the transverse cross-section of FSW joints, focusing on grain and precipitate features in different regions of the joints by optical microscope (OM), electron back scattered diffraction (EBSD) and transmission electron microscope (TEM) technologies. The specimens for OM observation were prepared by grinding and then polishing, and etching by Keller's reagents (2 ml hydrofluoric acid, 3 ml hydrochloric acid, 5 ml nitric acid and 190 ml water) at last. The EBSD specimens were prepared by grinding and mechanical polishing, and then electro-polishing with a

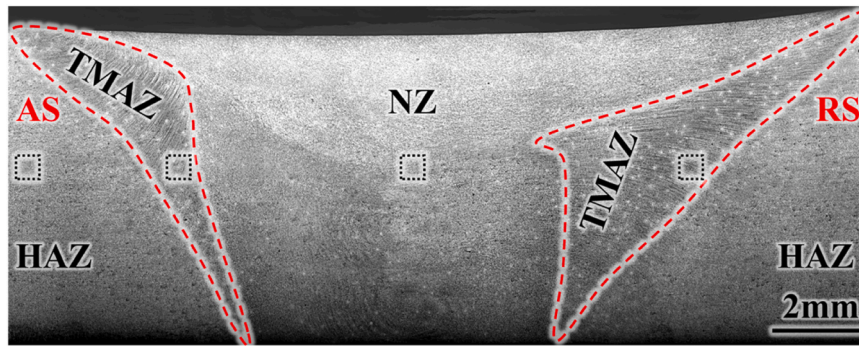


Fig. 1. Macroscopic morphology of FSW joints and the different regions of joints for microstructure analysis marked by boxes (AS-HAZ, AS-TMAZ, NZ and RS-TMAZ).

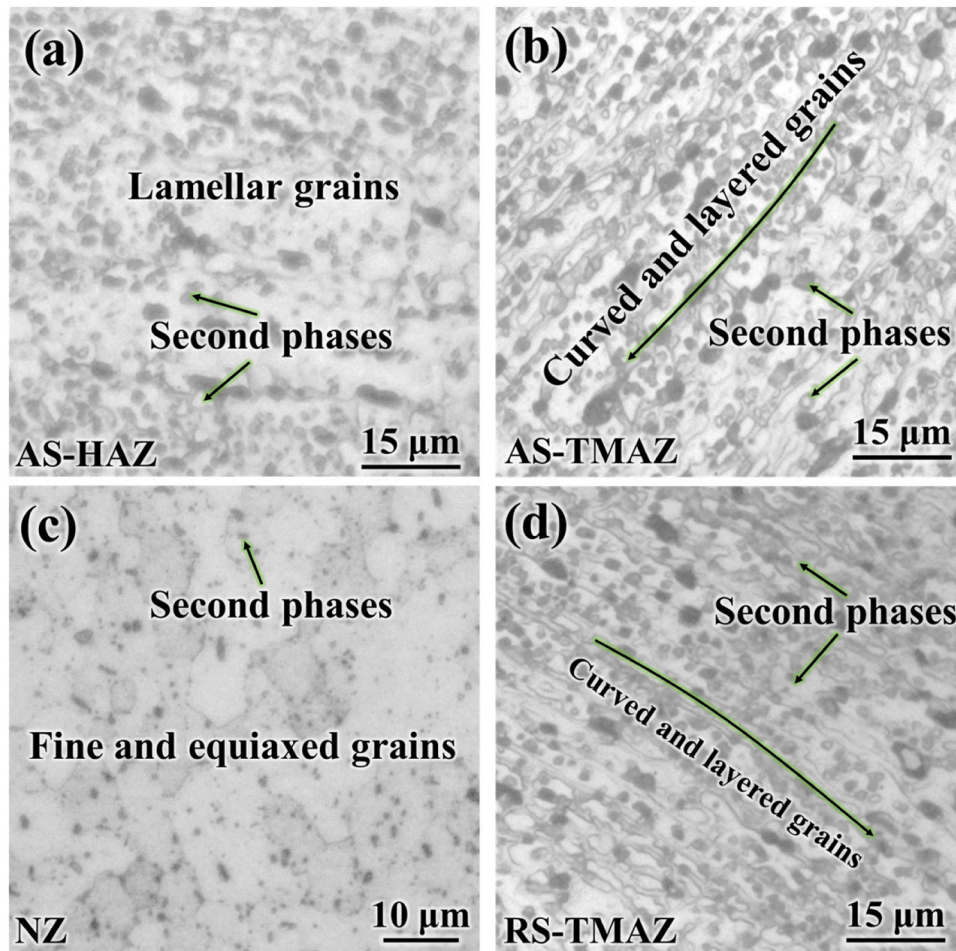


Fig. 2. Optical microscopy (OM) images of different regions of the FSW joints: (a) AS-HAZ, (b) AS-TMAZ, (c) NZ, (d) RS-TMAZ.

mixture of 10 % HClO_4 and 90 % $\text{C}_2\text{H}_5\text{OH}$ for 120 s at 20 V and -20°C . EBSD test was carried out on a scanning electron microscope (SEM, Zeiss Auriga) with an operating voltage of 20 kV, and the EBSD scanning step size was performed on 0.3 μm or 1 μm . EBSD data was processed by Aztec-Crystal software. Various colors appear in EBSD maps representing different crystallographic directions which can reference the IPF coloring scheme. The low angle grain boundaries (LAGBs) with misorientation angles between 2° and 15° were illustrated with white lines, while the high angle grain boundaries (HAGBs) with misorientation angles above 15° were noted by black lines. Precipitates of welding joints were characterized by back scattered electron (BSE, Zeiss Auriga

SEM) and transmission electron microscopy (TEM, Talos F200S). The samples for BSE observation were prepared by mechanical grinding and polishing. The TEM samples were obtained by twin-jet electro-polishing with a solution of 70 % CH_3OH and 30 % HNO_3 at 15 V and -30°C .

Mechanical properties of the FSW joints were studied by MH-5L micro-hardness testers and AG-X tensile test machines. Micro-hardness profiles were measured on the transverse cross-section of FSW joints micro-hardness testers. The measurement was carried out in the middle thickness of joints with an interval of 0.5 mm under a load of 500 g for 10 s. Tensile test specimens were prepared as per ASTM: E8- M11 guidelines in which the room-temperature tensile tests were carried out

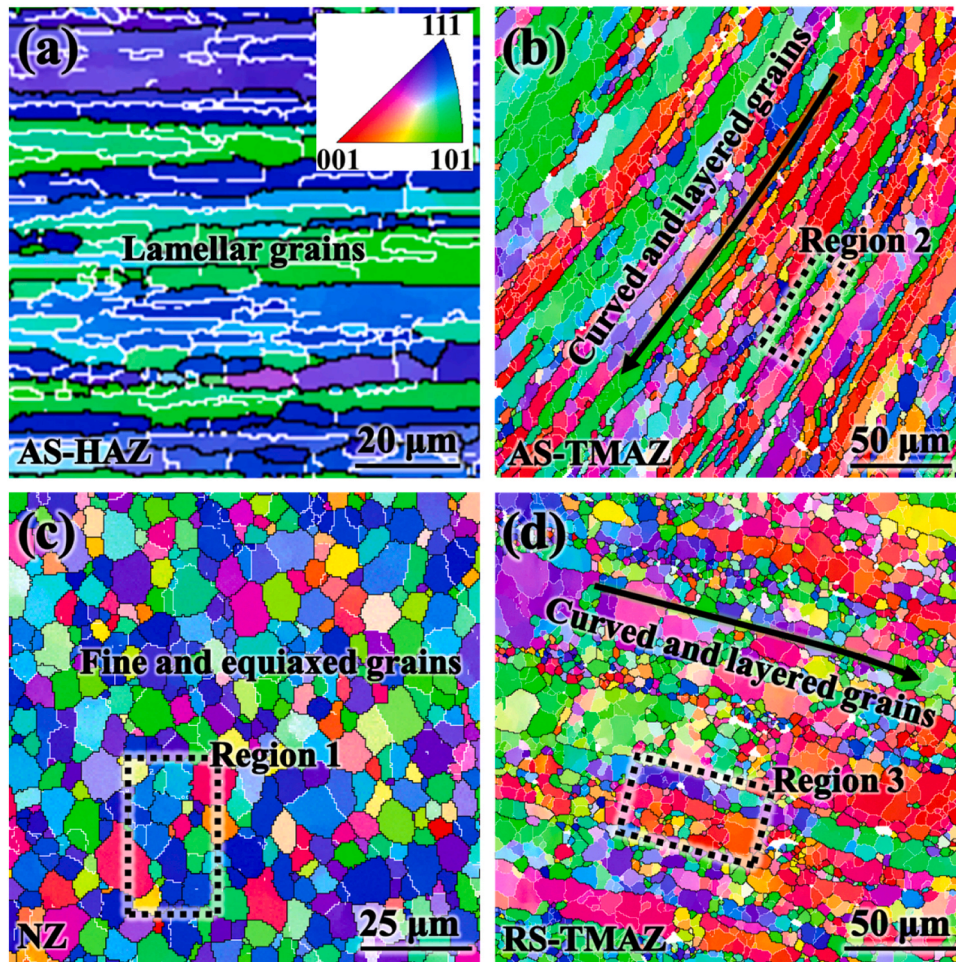


Fig. 3. Inverse pole figure (IPF) of different regions of the FSW joints: (a) AS-HAZ, (b) AS-TMAZ, (c) NZ, (d) RS-TMAZ.

with a displacement state of 1 mm/min, and three samples were tested for each condition. Fracture morphologies of the tensile samples were analyzed using Zeiss Auriga FIB-SEM.

3. Results and discussion

3.1. Microstructural features

Fig. 1 shows the macroscopic morphology of the cross-section of Al-Cu-Li alloy FSW joints. It can be found that typical regions, i.e., the HAZ, TMAZ and NZ, were observed in the joints. The microstructural characteristics of these regions were characterized by optical microscopy (OM) and EBSD analysis, as shown in Figs. 2–7.

As can be seen from the OM images (Fig. 2), the HAZ is dominated by lamellar elongated grains, the AS-TMAZ and RS-TMAZ are mainly curved layered grains, while the NZ is mainly fine equiaxed grains. In this study, the Al-Cu-Li alloy was rolled, and the grains were in lamellar elongated structure. In the FSW, the HAZ is mainly affected by the welding thermal cycle, and the recovery process occurs, and the grain morphology remains similar to that of the BM. The TMAZ is subjected to the joint action of welding thermal cycling and plastic deformation stress in the welding zone, the original long grain is bent and deformed, and some dynamic recrystallization occurs at the same time, resulting in a few fine recrystallization grains. The NZ was subjected to severe plastic deformation and high welding temperature, and completely dynamic recrystallization occurred, resulting in a large number of fine equiaxed grains.

In addition, there are a large number of coarse second phases in the

HAZ, AS-TMAZ and RS-TMAZ, while these precipitates basically disappear in the NZ. After the complete annealing treatment of the BM, a large number of coarse equilibrium phases are formed, and the intense thermomechanical action of FSW causes these precipitates to dissolve, so the coarse precipitates are rarely observed in NZ. The thermomechanical action of HAZ and TMAZ is relatively small and fails to dissolve these equilibrium phases, so a large amount of coarse precipitated phase is still retained.

In the Fig. 3, it can be found that grains in the AS-HAZ is mainly in (111) and (101) orientation, and more (001) orientation is generated in the TMAZ. While, grains in the NZ shows random orientation. Grains morphologies of these regions are similar to what observed in the OM (Fig. 2), indicating that the fine and equiaxed recrystallization grains are observed in the NZ and TMAZ. Fig. 4 shows the distribution characteristics of LAGBs and HAGBs in each region of the joint. Through quantitative analysis, it is found that the content of LAGBs of HAZ is the highest, which is 52.4, as shown in Fig. 5. The content of LAGBs in TMAZ decreased slightly, with AS-TMAZ being 50.8 % and RS-TMAZ being 42.7. The content of LAGBs in NZ is the lowest (15.7 %).

Generally, stress induces plastic deformation in materials, changing grain morphology and orientation, while high temperatures promote recrystallization. FSW is a complex thermomechanical process where the material near the weld zone experiences dynamic recrystallization due to severe plastic deformation and high-temperature during welding. In the FSW joint, the thermomechanical impact is strongest in the NZ. Intense mechanical stirring and high-temperature there enable complete recrystallization, reducing the density of LAGBs and dislocations, as seen in Figs. 4 and 6. In the TMAZ, the thermomechanical action is weaker,

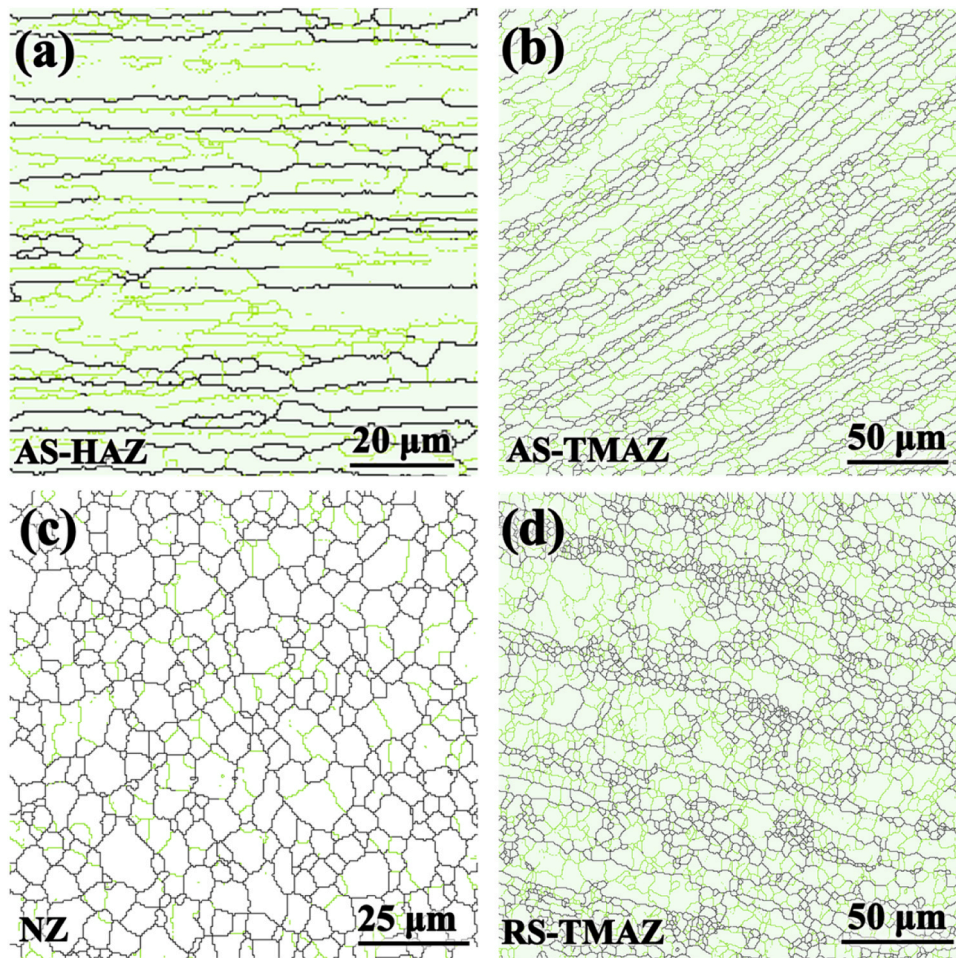


Fig. 4. Grain boundaries distribution of different regions of the FSW joints: (a) AS-HAZ, (b) AS-TMAZ, (c) NZ, (d) RS-TMAZ.

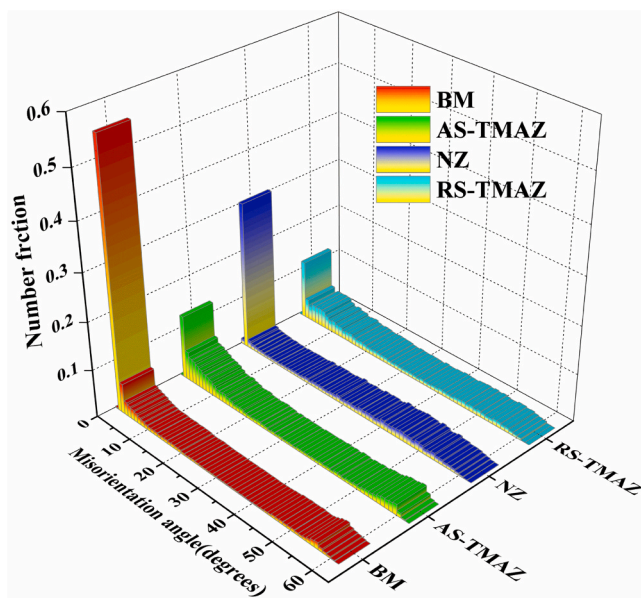


Fig. 5. Comparison of misorientation angle distributions of grains in different regions of the joints.

causing partial dynamic recrystallization. Although fine recrystallized grains form, many deformed structures like LAGBs and dislocations remain, leading to a relatively high content of them in TMAZ. The AS-TMAZ has more elongated grains than the RS-TMAZ, because the former undergoes more severe thermomechanical forces during FSW.

FSW's heat and force variations result in different dynamic recrystallization mechanisms. The NZ shows features of continuous (CDRX) and discontinuous (DDR) dynamic recrystallization. In DDR, new strain-free grains nucleate at deformed areas. The TMAZ has traces of geometric dynamic recrystallization (GDRX) besides CDRX and DDR, as shown in Fig. 7.

3.2. Hardness profiles

Micro-hardness profiles of the Al-Cu-Li alloy FSW joints are shown in Fig. 8. After FSW, the material in the weld and its vicinity is strengthened, the hardness increases, and the overall hardness distribution curve of the joint becomes “n” type. In addition, the region with the largest increase in hardness was AS-NZ, reaching 125.2 HV. From AS-NZ to RS-NZ, the increment of hardness in the NZ gradually decreases, with a minimum hardness of about 69.8 HV (increasing 19.3 HV). The increase in hardness of TMAZ is relatively small, about 2–28.5 HV, and the increase in hardness of AS-TMAZ is more. The hardness of the heat affected zone is consistent with that of the base material, with no increase, about 50.5 HV.

Generally, hardness profiles appear mostly in “W” shape in the FSW joints of precipitation strengthening Al alloys [6,24]. However, hardness curves of the joints can be different, resulting from the varied welding

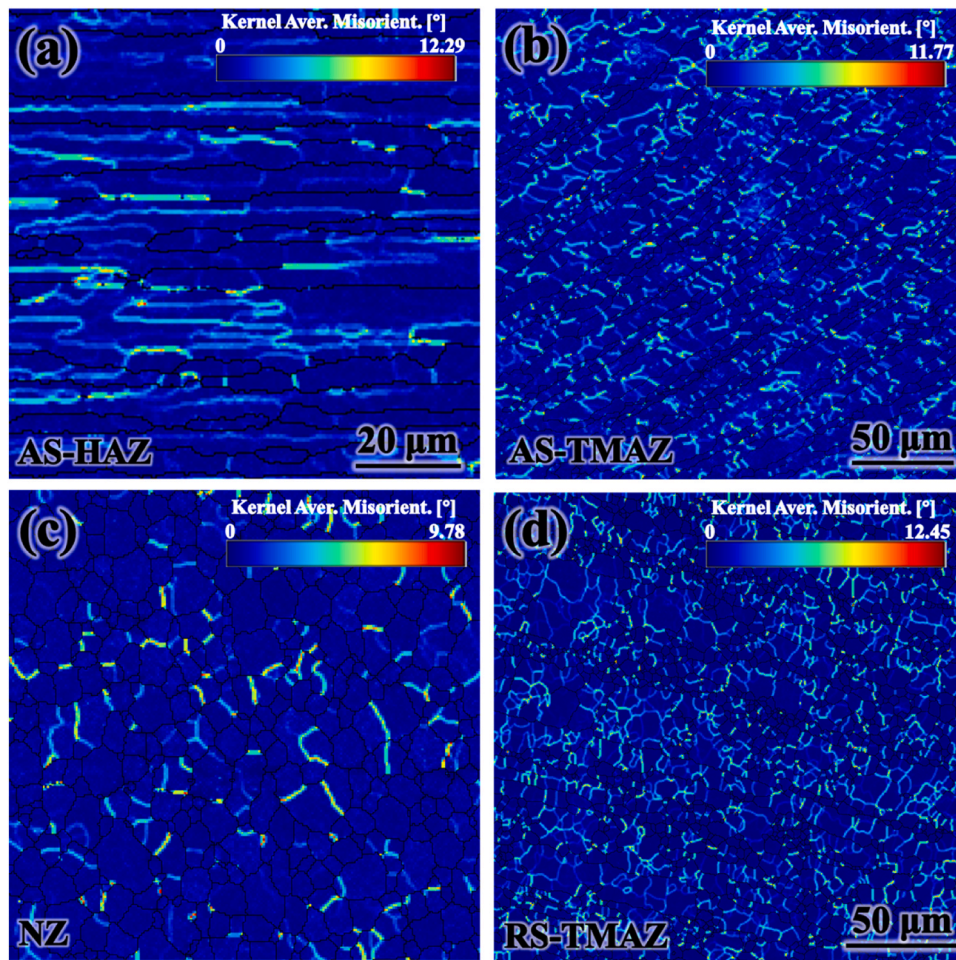


Fig. 6. Kernel average misorientation (KAM) maps of grains in different regions of the FSW joints: (a) AS-HAZ, (b) AS-TMAZ, (c) NZ, (d) RS-TMAZ.

condition, such as thickness of welding plates, cooling process and original status of base materials [25–28]. In this study, the first two factors are relatively routine, only the status of the material is different from that reported in most literature. The BM was in ‘O’ condition which involved an annealing at 400 °C for sufficient time, with the effect of strain hardening vanishing completely. It is well known that Al-Cu-Li alloy is a kind of typical precipitation strengthening Al alloy, whose mechanical properties are mainly determined by precipitates [2,3]. Dissolution, coarsening and precipitation of precipitates are caused by severe plastic deformation and sufficient heat input during friction stir welding process, significantly affecting hardness distribution of welding joints [5,29–31]. Thus, precipitate features of the FSW joints will be analyzed in detail.

3.3. Precipitates characterization

Fig. 9 shows the distribution of secondary phases in different regions of the joints using SEM-BSE analysis. A lot of coarse secondary phases are observed in the HAZ and TMAZ, which are mostly distributed along grain boundaries. While, obviously smaller and less of these phases can be found in the NZ. To further analyze the distribution patterns of phases in different regions of the joints, Transmission Electron Microscopy (TEM) was employed for precipitate analysis, as shown in Figs. 10–13. It should be noted that in the TEM analysis, the schematic diagrams of different regions are presented in the upper-right corner of each figure, for example, Fig. 10a.

3.3.1. Phases in the BM-HAZ

Fig. 10 shows the distribution characteristics of phases in the BM or the HAZ. It can be found that a large number of coarse precipitates distributed along grain boundaries exist in these two regions, while a small amount of spherical precipitates exist within the grain inners. In the SAED diagram, only the diffraction spots of Al matrix are observed, and there is no diffraction information of phase, indicating that there is no coherent relationship between these coarse precipitated phases and Al matrix. It is known from the literature that these fine spherical precipitated phases are δ' (Al_3Li) and β' (Al_3Zr), and their diffraction information is difficult to observe because of their small content and size. At the same time, because δ' and β' are very close to each other in crystal structure, lattice constant, and orientation relationship with Al matrix, they are usually expressed as δ'/β' in Al-Cu-Li alloys. Through STEM-EDS analysis of these coarse precipitates, the enrichment of elements such as Al, Cu, Mg and Ag can be obviously observed. It can be noted that in a fully annealed Al-Cu-Li alloy, these precipitates should be an equilibrium of Al, Cu, Mg, and Li (too light to be detected). Chen et al. suggests that these equilibrium phases may be Al_2Cu (θ), $\text{Al}_{7.5}\text{Cu}_4\text{Li}$ (T_B), Al_6CuLi_3 (T_2) and Al_6CuMg_4 (T) [17]. The generation of these coarse phases which costs a lot of solutes creates the microstructure significantly devoid of strengthening particles in both of the matrix and grain boundaries [32]. Thus, the BM was developed as a weakening state with low hardness. The spherical particles of δ' and β' are mainly precipitated during nature aging process [6,9,10,33].

Generally, a weak zone with the lowest hardness, resulting from the dissolution and coarsening of precipitates, is always detected in the HAZ [7,11,34]. However, in this study, no significant hardness difference was

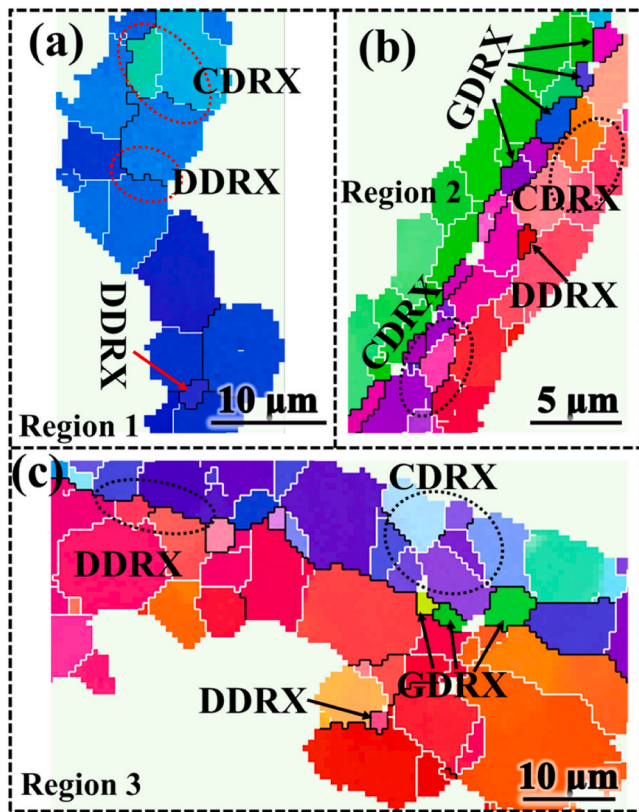


Fig. 7. Selected grains for analyzing dynamic recrystallization behavior in different regions of the FSW joints: (a) NZ, (b) AS-TMAZ, (c) RS-TMAZ.

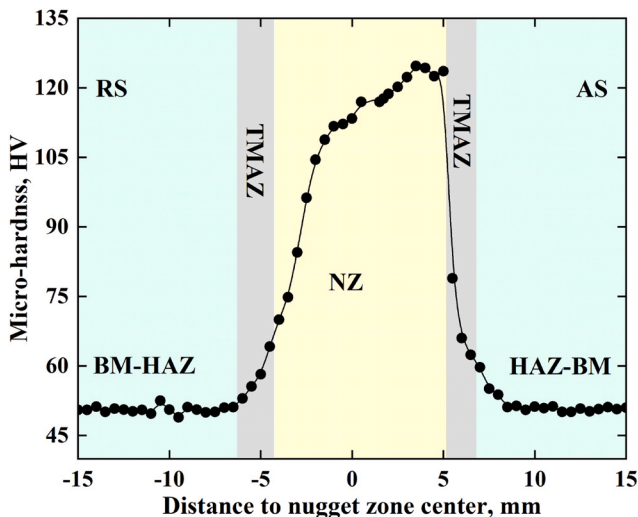


Fig. 8. Hardness profiles on cross-section of the FSW joints.

detected between the HAZ and the BM. This indicates that the welding thermal cycle had a negligible impact on the precipitates in the HAZ. The BM, having undergone long-term high-temperature heat treatment, had only a small number of solutes and strengthening particles remaining in the matrix, with most solutes having transformed into equilibrium phases. The limited welding temperature was insufficient to promote the precipitation and coarsening of strengthening precipitates. Consequently, the phase characteristics in the HAZ were consistent with those of the BM, leading to a similar hardness value between the HAZ and the BM.

3.3.2. Phases in the TMAZ

Fig. 11 presents the TEM analysis results of phases in the AS-TMAZ and RS-TMAZ. It is evident that the distribution characteristics of phases in these two regions are essentially identical. Specifically, the coarse equilibrium phase is predominantly distributed along the grain boundaries of the curved grains. Moreover, within the grain interior, there are numerous entangled dislocations. In the SAED patterns, only the diffraction information of the Al matrix is observed. During the FSW process, the TMAZ experiences a relatively high plastic deformation (extrusion, shearing and forging) and welding temperature, leading to the dissolution, precipitation and coarsening of precipitates [5]. Generally, the maximum temperature of TMAZ is about 400°C. However, in this research, the coarse secondary phases were not decreased obviously due to the insufficient strain and heat input during the welding. This is because the temperature is not high enough for the coarse equilibrium phase to dissolve. The thermal cycling in the TMAZ had limited effect on coarse phases, but were enough for the dissolution of tiny dispersoids promoting the re-precipitation of the δ' phases and the development of β' phases in the subsequent cooling process. The δ' phase is easy to form at relatively low temperature (less than 100 °C) due to low activation and interfacial energy [3]. The β' phases prefer to precipitate on dislocations and grain boundaries, which can also act as nucleation sites for δ' precipitates [33]. Hence, the high density of dislocations and heat input jointly promoted the generation of more δ' and β' precipitates. Thus, a little increase in hardness, resulting from the content of the fine precipitates, was only detected in the AS-TMAZ. The thermomechanical action during FSW makes the deformed grains in the TMAZ. As a result, the orientation of the phases along the grain boundaries of these grains changes accordingly. Given the relatively low degree of recrystallization in TMAZ, a substantial amount of residual strain remains in the matrix in the form of dislocations.

3.3.3. Phases in the NZ

In most FSW studies of Al alloys, the hardness distribution in the NZ generally exhibits a smooth wavy curve, indicating that the hardness values of small areas within the NZ are relatively similar. Nevertheless, in the present study, the hardness in different regions of the NZ varies considerably. Specifically, the hardness values display a decreasing trend from the advancing-side (AS-NZ) to the retreating-side (RS-NZ) of the NZ.

The Al-Cu-Li alloy is a precipitation-strengthened aluminum alloy, and its mechanical properties are predominantly related to the distribution of the precipitated phase. To disclose the distribution characteristics of the precipitated phase in the NZ, TEM analysis was conducted on the AS-NZ, central region of the NZ (NCZ), and RS-NZ, as shown in Fig. 12.

As can be seen from Fig. 12, the grains in different regions of the NZ are fine and equiaxed. Fine δ' / β' phases and dislocations are detected in all three regions. In the AS-NZ, no obvious grain-boundary precipitates are observed. In the NCZ, more relatively small-sized grain-boundary precipitates (approximately 0.5 μm) are found, and a significant number of precipitates of the same size are also present inside the grains. However, in the RS-NZ, coarse grain-boundary precipitates, with a size of about 1–2 μm , are frequently observed.

The NZ suffers severe plastic deformation and high thermal exposure during FSW process [12]. Some researchers estimated that effective strains in this region exceeded 40 at a high strain rates (about 10 s^{-1}) [36]. The maximum temperature could approach about 0.8 T_m , or even 0.95 T_m in Al alloys [5]. Fine equiaxed grains are developed in this region due to dynamic recrystallization [37]. The dissolution, precipitation coarsening and fragmentation of precipitates, resulting from dramatic thermal-mechanically process, can also be found [38]. In this study, dynamic recrystallization was developed in the whole NZ, leading to the generation of fine recrystallization grains. However, precipitate features were evidently different in the individual regions of the NZ, indicating that coarse phases were absent in the AS-NZ but were still

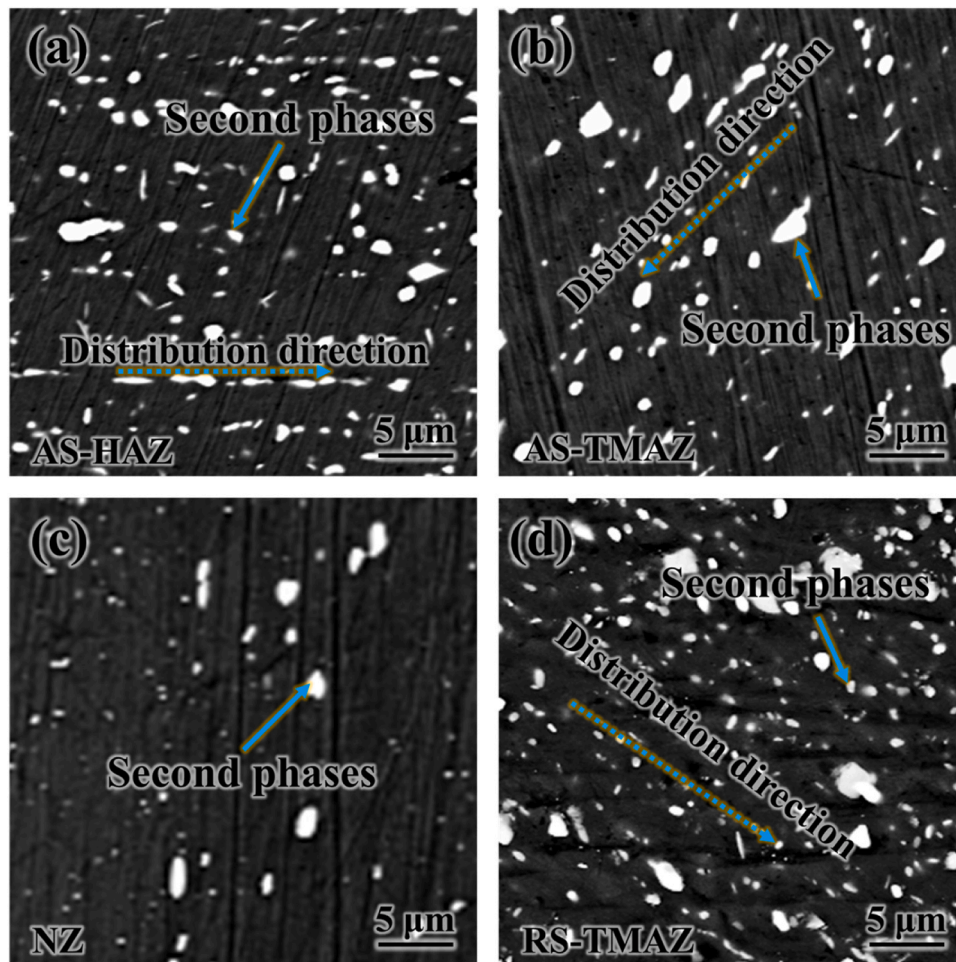


Fig. 9. SEM-BSE characterization of the second phases in different regions of joints: (a) AS-HAZ, (b) AS-TMAZ, (c) NZ, (d) RS-TMAZ.

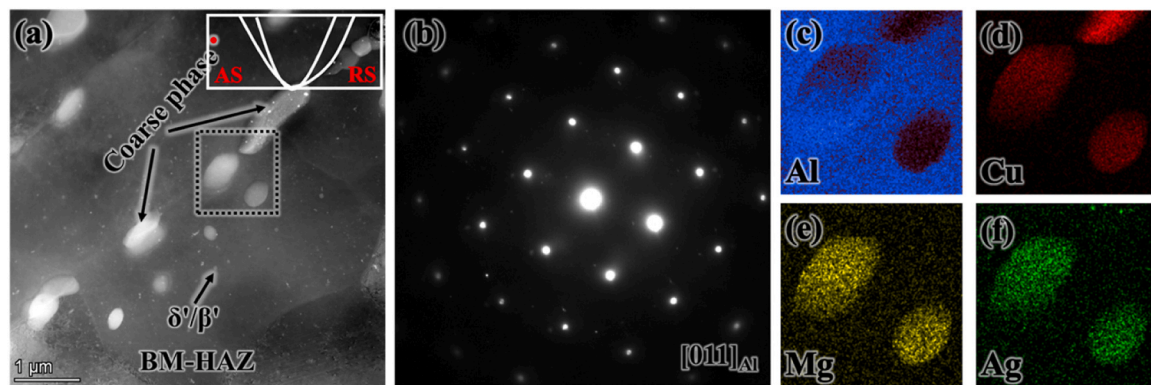


Fig. 10. TEM analysis of precipitates of the BM-HAZ along $[35]_{\text{Al}}$ axis: (a) STEM-DF maps, (b) corresponding SAED images of (a), (c–f) the corresponding EDS mappings of the box in (a).

observed in the RS-NZ. Furthermore, the coarse precipitates in the RS-NZ were smaller than those in the BM. These differences might be caused by the development of heterogeneous thermal-mechanical history.

In this study, the BM is a fully annealed Al alloy. Most of its solute atoms precipitate fully at the grain boundaries, forming coarse equilibrium phases. As a result, the hardness of the alloy is low. The thermomechanical action of the FSW can redissolve the phases in the weld zone. The solute atoms then dissolve into the matrix, achieving solid-solution strengthening. Consequently, the hardness of the NZ is higher

than that of the BM and the he HAZ. Since FSW is a complex and non-uniform thermomechanical process, the thermomechanical effects on different regions of the weld zone vary. Previous studies [17] have indicated that the material in the AS-NZ is mainly subjected to the shear action of the stirring pin, while the material in the RS-NZ is mainly under extrusion. This leads to more intense thermomechanical action in the former and less in the latter.

The intense rotational-shear action of the stirring pin causes the original coarse phases in the NZ region to fragment and dissolve. The AS-NZ experiences the most significant thermomechanical action. The

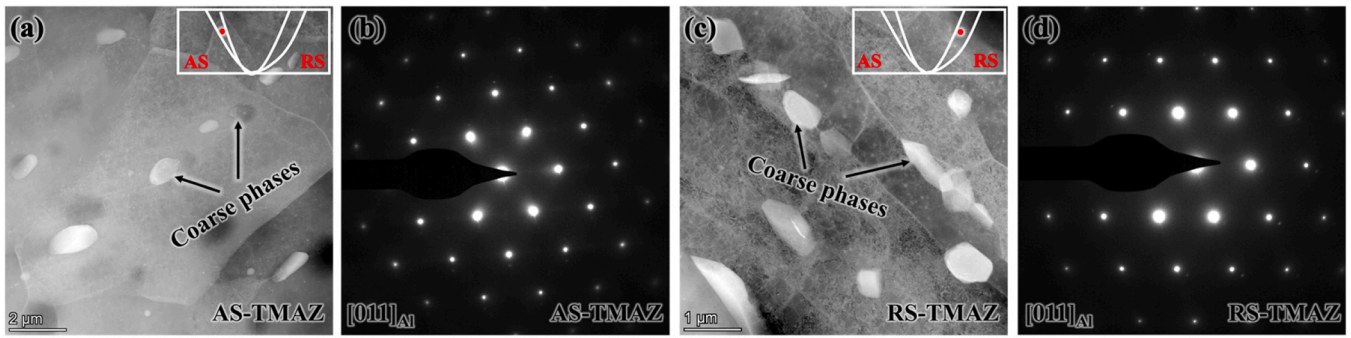


Fig. 11. TEM analysis of precipitates of the AS-TMAZ and RS-TMAZ along $[35]_{Al}$ axis: (a) STEM-DF maps of AS-TMAZ, (b) corresponding SAED images of (a), (c) STEM-DF maps of RS-TMAZ, (d) corresponding SAED images of (c).

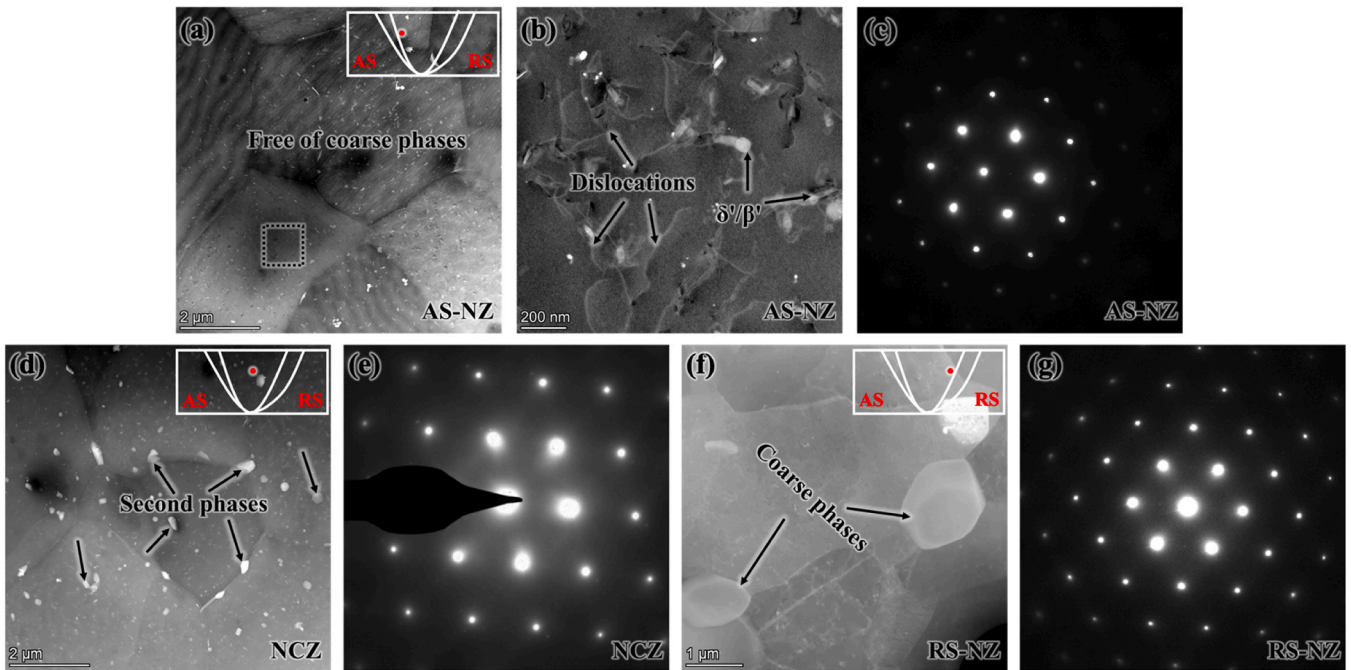


Fig. 12. TEM analysis of precipitates of the NZ along $[35]_{Al}$ axis: (a-c) AS-NZ, (d, e) NCZ, (f, g) RS-NZ.

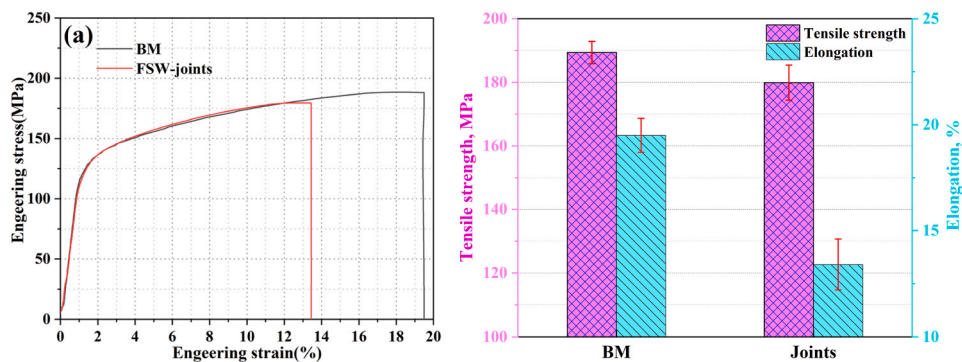


Fig. 13. Tensile test results of the BM and FSW joints: (a) Engineering stress-strain curves, (b) Tensile properties.

original equilibrium phases are fully dissolved and almost disappear, resulting in the maximum solid-solution strengthening effect and the highest hardness. The thermomechanical action on the central region of the NCZ is less intense than that on the AS-NZ. The equilibrium phases partially dissolve, and the size of the remaining equilibrium phases decreases significantly, leading to a reduced solid-solution strengthening

effect. The thermomechanical action on the RS-NZ is evidently smaller than that on the AS-NZ and NCZ. The degree of dissolution of the original equilibrium phases is lower, and the corresponding solid-solution strengthening effect is also weaker. Therefore, more equilibrium phases with larger sizes are observed in RS-NZ.

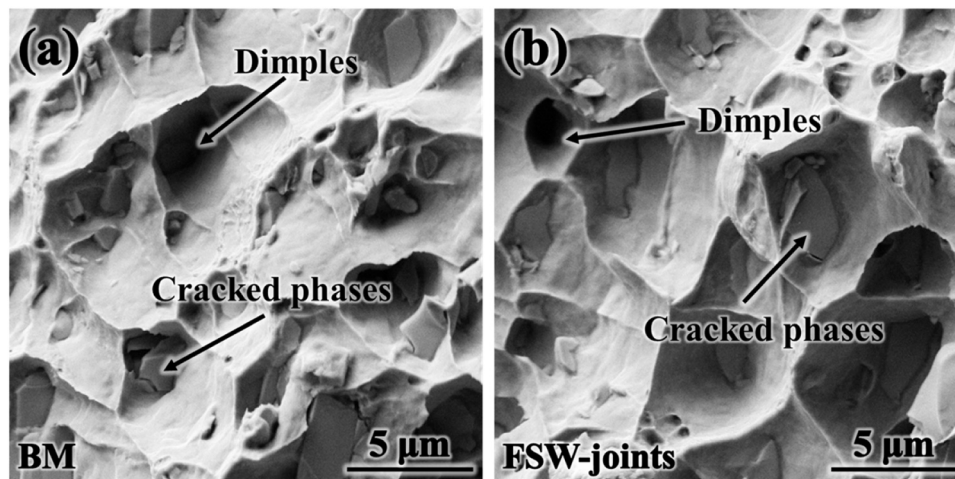


Fig. 14. SEM analysis of fracture morphologies of (a) the BM and (b) the FSW joints.

3.4. Tensile properties of the joints

Fig. 13 presents a comparison of the tensile properties between the BM and the FSW joints. The strength of the BM is measured to be 189.4 MPa, with an elongation after fracture of 19.5 %. The maximum tensile strength of the FSW joints reaches 179.9 MPa, approximately 95.0 % of the BM, and the elongation after fracture is 13.4 %, about 68.7 % of the BM. Evidently, after FSW, the strength of the fully-annealed Al-Cu-Li alloy experiences a minor decrease, while the elongation after fracture drops significantly. Additionally, the tensile fracture of the FSW joints occurs in the HAZ and BM regions, and the tensile fracture morphologies of the BM and FSW joints are illustrated in Fig. 14. It can be observed that the fracture morphologies of the BM and FSW joints are highly similar, with a large number of ductile fracture features such as dimples, indicating that the fracture mechanism of both is ductile fracture.

In previous studies [20,39,40], the strength of FSW joints was notably reduced, typically dropping to 60–70 % of the BM. This is because in those studies, artificially aged aluminum alloys were mainly employed as the BM. The welding thermal cycle led to significant dissolution and coarsening of the strengthening phases, resulting in a substantial decline in the joint strength. In this study, the BM is a fully-annealed aluminum alloy. The thermomechanical action of FSW mainly causes the phases to break down and dissolve, thereby enhancing the strength, and the strengthened area is primarily concentrated in the NZ. Consequently, during the tensile test of FSW joints, tensile deformation is more likely to occur in the softer regions (the HAZ and BM) of the sample. As the tensile deformation progresses continuously, tensile stress gradually accumulates at the grain boundaries of the HAZ and BM and at the interface between the coarse precipitates and the Al matrix, ultimately leading to tensile fracture of the joint in these regions. Notably, the microstructures of the fractured HAZ and BM are very similar, and their mechanical properties are also quite alike, so the strength of the FSW joint is very close to that of the BM. However, the microstructure of the NZ and its adjacent areas changes considerably, and the overall microstructure uniformity of the FSW joint decreases, resulting in a reduction in the joint's uniform deformation ability. Thus, the elongation after fracture of the joint is significantly lower than that of the base material.

Compared with previous literature, it is evident that when using fully-annealed Al-Cu-Li alloy for FSW, the mechanical properties of the joint change minimally, especially the joint strength with the slightest variation, and the local area of the joint is strengthened. As is well-known, the fully-annealed aluminum alloy is in an intermediate state of the production process and can be followed by complex thermal

processing. Therefore, if this material is selected for FSW and appropriate post-welding heat treatment is applied, a workpiece with excellent comprehensive performance can be obtained, and such a processing program is also consistent with the production process of complex parts.

4. Conclusion

In this paper, microstructure and mechanical properties of the friction stir welded full annealing condition Al-Cu-Li alloys are studied. Evolution mechanisms of grains and precipitates are discussed in detail, and the correlation of microstructure, mechanical properties and fracture mechanism of the joints are established. The main conclusions can be drawn as follows:

- (1) Finely equiaxed grains with random orientation develop in the NZ due to occurrence of DDRX and CDRX. Equiaxed grains and sub-structured grains with more (001) orientation are observed in the TMAZ owing to the development of DDRX, CDRX and GDRX. The NZ experiences sufficient DRX, resulting the lowest dislocation density and LAGBs. While the TMAZ mainly suffers partial DRX, generating deformed long grains with more dislocation and LAGBs. The HAZ has similar microstructure characteristics, such as grain morphology and orientation, dislocation density and LAGBs content, to the BM.
- (2) The phase characteristics of the HAZ, TMAZ, and BM are essentially identical. Specifically, a large number of coarse equilibrium phases are present along the grain boundaries, leading to low hardness in these regions. In the NZ, these equilibrium phases dissolve, exhibiting an obvious solid-solution strengthening effect and thus increasing the hardness of the NZ. In the AS-NZ, these precipitates are completely dissolved. In the NCZ, the size and quantity of phases decrease significantly, both of which slightly change in the RS-NZ. As a result, the solid-solution strengthening effect in these three regions decreases successively, and the overall hardness of the joint presents an “n”-type distribution.
- (3) When the fully-annealed Al-Cu-Li alloys is subjected to FSW, both the strength and plasticity of this alloy are lower than those of the BM. The strength of the BM is 189.4 MPa, while that of the joints is 179.9 MPa, with a joint coefficient of 95.0 %. Numerous dimples are present in the tensile fractures of both the joints and the BM, indicating distinct ductile-fracture characteristics. The significant changes in the grain structure and phases near the NZ result in a reduction in the overall uniform-deformation ability of the joint. Consequently, the elongation of the joint after fracture is evidently lower than that of the base material.

CRediT authorship contribution statement

Jie Wang: Validation, Methodology, Investigation. **Zhiqing Zhang:** Resources, Project administration. **Wenhao Chen:** Validation, Methodology, Investigation. **Peng Chen:** Writing – review & editing, Writing – original draft, Project administration, Methodology, Investigation, Funding acquisition, Conceptualization. **Meizi Tian:** Methodology, Formal analysis, Data curation. **Ge Liu:** Writing – original draft, Resources, Investigation, Funding acquisition, Conceptualization.

Declaration of Competing Interest

We would like to submit the enclosed manuscript entitled “Microstructure and mechanical properties of friction stir welded full annealing condition Al-Cu-Li alloys”, which we wish to be considered for publication in the journal of *Materials Today Communications*.

No conflict of interest exists in the submission of this manuscript, and manuscript is approved by all authors for publication. I would like to declare on behalf of my co-authors that the work described was original research that has not been published previously, and not under consideration for publication elsewhere, in whole or in part. All the authors listed have approved the manuscript that is enclosed.

Acknowledgements

This research is financially supported by Scientific and Technological Research Program of Chongqing Municipal Education Commission (KJQN202201436), Postdoctoral Research Project Special Fund in Sichuan Province and Natural Science Starting Project of SWPU (2023QZH017).

Data availability

Data will be made available on request.

References

- [1] D. Li, H. Liu, S. Du, et al., Insight on ultrasonic effect of Al Cu aluminum alloy joints fabricated by ultrasonic assisted non-thinning and penetrating friction stir welding, *Mater. Charact.* 207 (2024) 113605.
- [2] J.H. Kim, J.H. Jeun, H.J. Chun, et al., Effect of precipitates on mechanical properties of AA2195, *J. Alloy. Compd.* 669 (2016) 187–198.
- [3] R. Mishra, H. Sidhar, *Friction Stir Welding of 2xxx Aluminum Alloys Including Al-Li Alloys*, 1st ed, Butterworth-Heinemann, Waltham, MA, USA, 2016 (ISBN 978-0-12-805368-3).
- [4] G. Sun, W. Sun, L. Zhou, et al., Microstructure, mechanical and fracture properties of friction stir welded 2195 Al-Li alloy joints, *Chin. J. Aeronaut.* 37 (1) (2024) 345–361.
- [5] Z.Y. Ma, A.H. Feng, D.L. Chen, et al., Recent advances in friction stir welding/processing of aluminum alloys: microstructural evolution and mechanical properties, *Crit. Rev. Solid State* 43 (2017) 269–333.
- [6] H. Qin, H. Zhang, H. Wu, The evolution of precipitation and microstructure in friction stir welded 2195-T8 Al-Li alloy, *Mater. Sci. Eng. A* 626 (2015) 322–329.
- [7] A.K. Shukla, W.A. Baeslack, Study of process/structure/property relationships in friction stir welded thin sheet Al-Cu-Li alloy, *Sci. Technol. Weld. Join.* 14 (2013) 376–387.
- [8] G. Oertelt, S.S. Babu, S.A. David, et al., Effect of thermal cycling on friction stir welds of 2195 aluminum alloy, *Weld. J.* 80 (2001) 71–79.
- [9] R.W. Fonda, J.F. Bingert, Precipitation and grain refinement in a 2195 Al friction stir weld, *Metall. Mater. Trans. A* 37 (2006) 3593–3604.
- [10] J.A. Schneider, A.C. Nunes, P.S. Chen, et al., TEM study of the FSW nugget in AA2195-T81, *J. Mater. Sci.* 40 (2005) 4341–4345.
- [11] A.K. Shukla, W.A. Baeslack, Study of microstructural evolution in friction-stir welded thin-sheet Al-Cu-Li alloy using transmission-electron microscopy, *Scr. Mater.* 56 (2007) 513–516.
- [12] R.S. Mishra, Z.Y. Ma, Friction stir welding and processing, *Mater. Sci. Eng. R* 50 (2005) 1–78.
- [13] X.C. Liu, Q. Wang, X.J. Pei, et al., Microstructural evolution of 6061-T6 aluminum alloy in vortex- friction stir welding, *Mater. Charact.* 195 (2023) 112544.
- [14] T.S. Liu, F. Qiu, H.Y. Yang, et al., Insights into the influences of nanoparticles on microstructure evolution mechanism and mechanical properties of friction-stir-welded Al 6061 alloys, *Mater. Sci. Eng. A* 871 (2023) 144929.
- [15] D. Li, H. Liu, S. Du, et al., Investigation on material flow and microstructural evolution mechanism in non-thinning and penetrating friction stir welded Al-Cu aluminum alloy, *Mater. Sci. Eng. A* 864 (2023) 144527.
- [16] K. Huang, R.E. Logé, A review of dynamic recrystallization phenomena in metallic materials, *Mater. Des.* 111 (2016) 548–574.
- [17] P. Chen, T.N. Li, X. Yin, et al., The precipitate evolution in friction stir welding of 2195-O Al-Li alloy, *J. Mater. Res. Technol.* 24 (2023) 1991–2006.
- [18] H. Sidhar, R.S. Mishra, Aging kinetics of friction stir welded Al-Cu-Li-Mg-Ag and Al-Cu-Li-Mg alloys, *Mater. Des.* 110 (2016) 60–71.
- [19] Z. Yu, J. Qiu, H. Li, et al., Microstructure, mechanical properties and thermal stability of friction-stir-processed Al-Cu-Mg-Ag alloy, *Mater. Sci. Eng. A* 863 (2023) 144525.
- [20] X. Guo, S.H. Wen, H.J. Jiao, et al., Effect of aging treatment on microstructure and mechanical properties of TIG welded joints of 2195-T8 Al-Li alloy, *Mater. Charact.* 196 (2023) 112576.
- [21] B. Mondal, S. Sinha, J. Reed, et al., Effect of backing plate on microstructure and properties of friction stir welded 2195-O alloy, *Scr. Mater.* 241 (2024) 115899.
- [22] J. Chen, R. Chen, H. Liao, et al., Improving joint performance of friction stir welded 2195-O Al-Li alloy by post-weld heat treatment and rolling deformation, *J. Mater. Res. Technol.* 29 (2024) 5048–5059.
- [23] P. Chen, J. Wang, W.H. Chen, et al., Influence of post-weld rolling and artificial aging on microstructure and mechanical properties of friction stir welded 2195-T4 Al-Li alloy joints, *Mater. Sci. Eng. A* 914 (2024) 147165.
- [24] F. Zhang, X. Su, Z. Chen, Z. Nie, Effect of welding parameters on microstructure and mechanical properties of friction stir welded joints of a super high strength Al-Zn-Mg-Cu aluminum alloy, *Mater. Des.* 67 (2015) 483–491.
- [25] H. Chen, L. Fu, P. Liang, et al., Defect features, texture and mechanical properties of friction stir welded lap joints of 2A97 Al-Li alloy thin sheets, *Mater. Charact.* 125 (2017) 160–173.
- [26] C. Yang, J.F. Zhang, G.N. Ma, et al., Microstructure and mechanical properties of double-side friction stir welded 6082Al ultra-thick plates, *J. Mater. Sci. Technol.* 41 (2020) 105–116.
- [27] W. Xu, J. Liu, G. Luan, C. Dong, Temperature evolution, microstructure and mechanical properties of friction stir welded thick 2219-O aluminum alloy joints, *Mater. Des.* 30 (2009) 1886–1893.
- [28] B. Malard, F. De Geuser, A. Deschamps, Microstructure distribution in an AA2050 T34 friction stir weld and its evolution during post-welding heat treatment, *Acta Met.* 101 (2015) 90–100.
- [29] M.X. Milagre, N.V. Mogili, U. Donatus, et al., On the microstructure characterization of the AA2098-T351 alloy welded by FSW, *Mater. Charact.* 140 (2018) 233–246.
- [30] H. Liu, Y. Hu, C. Dou, et al., An effect of the rotation speed on microstructure and mechanical properties of the friction stir welded 2060-T8 Al-Li alloy, *Mater. Charact.* 123 (2017) 9–19.
- [31] Y. Tao, Z. Zhang, B.H. Yu, et al., Friction stir welding of 2060-T8 Al-Li alloy. Part II: tensile fracture behavior, *Mater. Charact.* 168 (2020) 110507.
- [32] P.S. Chen, B.N. Bhat, Time-temperature-Precipitation behavior in Al-Li alloy 2195, *NASA Tech. Rep.* (2002) 211548.
- [33] K.S. Prasad, A.A. Gokhale, A.K. Mukhopadhyay, et al., On the formation of faceted Al_3Zr (β') precipitates in Al-Li-Cu-Mg-Zr alloys, *Acta Met.* 47 (8) (1999) 2581–2592.
- [34] Z. Zhang, B.L. Xiao, Z.Y. Ma, Hardness recovery mechanism in the heat-affected zone during long-term natural aging and its influence on the mechanical properties and fracture behavior of friction stir welded 2024Al-T351 joints, *Acta Met.* 73 (2014) 227–239.
- [35] C. Gu, X. Yang, W. Tang, et al., Softening behavior of stationary shoulder friction stir welded joint for thick-plate Al-Li-Cu alloy, *J. Mater. Res. Technol.* 20 (2022) 3008–3024.
- [36] J.Q. Su, T.W. Nelson, C.J. Sterling, Microstructure evolution during FSW/FSP of high strength aluminum alloys, *Mater. Sci. Eng. A* 405 (2005) 277–286.
- [37] R. Fonda, Development of grain structure during friction stir welding, *Scr. Mater.* 51 (2004) 243–248.
- [38] Y.C. Chen, J.C. Feng, H.J. Liu, Precipitate evolution in friction stir welding of 2219-T6 aluminum alloys, *Mater. Charact.* 60 (2009) 476–481.
- [39] C. Peng, C. Jing, Q. Siyi, et al., Friction stir welding joints of 2195-T8 Al-Li alloys: correlation of temperature evolution, microstructure and mechanical properties, *Mater. Sci. Eng. A* 823 (2021) 141501.
- [40] P. Chen, W. Chen, J. Chen, et al., Effect of base material temper condition on precipitate evolution and mechanical properties of 2195 Al Li alloy friction stir welding joints, *Mater. Charact.* 209 (2024) 113712.